Article

Not peer-reviewed version

Real-Time 3D Vision-Based Robotic Path Planning for Automated Adhesive Spraying on Lasted Uppers in Footwear Manufacturing

Ya-Yung Huang , Jun-Ting Lai , Hsien-Huang Wu *

Posted Date: 16 April 2025

doi: 10.20944/preprints202504.1336.v1

Keywords: 3D vision; adhesive spraying; robotic path planning; footwear manufacturing; automated gluing; lasted upper; UV inspection; laser triangulation

 doi:10.20944/preprints202504.1336.v1

Article

Real-Time 3D Vision-Based Robotic Path Planning for Automated Adhesive Spraying on Lasted Uppers in Footwear Manufacturing

Ya-Yung Huang [1], Jun-Ting Lai [2] and Hsien-Huang Wu [2,*]

[1] Graduate School of Engineering Science and Technology, National Yunlin University of Science and Technology, Douliou 64002, Taiwan

[2] Department of Electrical Engineering, National Yunlin University of Science and Technology, Douliou 64002, Taiwan

* Correspondence: wuhp@yuntech.edu.tw

Abstract: The automation of adhesive application in footwear manufacturing is challenging due to complex surface geometries and model variability. This study presents an integrated 3D vision-based robotic system for adhesive spraying on lasted uppers. A triangulation-based scanning setup reconstructs each upper into a high-resolution point cloud, enabling customized spraying path planning. A six-axis robotic arm executes the path using an adaptive transformation matrix that aligns with surface normals. UV fluorescent dye and inspection are used to verify adhesive coverage. Experimental results confirm high repeatability and precision, with most deviations within the industry-accepted ±1 mm range. While localized glue-deficient areas were observed around high-curvature regions such as the toe cap, these remain limited and serve as a basis for further system enhancement. The system significantly reduces labor dependency and material waste while improving production efficiency. It has been successfully installed and validated on a production line in Hanoi, Vietnam, meeting real-world industrial requirements. This research contributes to advancing intelligent footwear manufacturing by integrating 3D vision, robotic motion control, and automation technologies.

Keywords: 3D vision; adhesive spraying; robotic path planning; footwear manufacturing; automated gluing; lasted upper; UV inspection; laser triangulation

1. Introduction

In the footwear industry remains one of the most labor-intensive sectors in global manufacturing, relying heavily on skilled manual labor to manage complex processes such as adhesive application on shoe uppers [1]. Although the trend toward automation has transformed many manufacturing sectors, the transition has been significantly slower in footwear production due to the use of flexible and deformable materials, including textiles, leather, and synthetic fabrics. These materials are difficult to handle with robotic systems because they are prone to shifting or warping, and they require high levels of dexterity and adaptability—qualities still challenging for most automation systems.

Projects such as ROBOFOOT have highlighted the technical and operational challenges that hinder full-scale automation in shoemaking [2]. Past industrial attempts, such as a major project in Mexico [3], ultimately failed due to difficulties in managing deformable materials and accommodating diverse shoe geometries in automated systems. As a result, researchers have increasingly focused on partial automation of specific manufacturing steps—particularly roughing and gluing—where robotic systems can offer tangible productivity and consistency gains. However, these applications require accurate trajectory information tailored to the type, size, and geometry of each shoe to control robotic paths effectively.

 doi:10.20944/preprints202504.1336.v1

Several approaches have been developed to extract gluing trajectories, including CAD-based offline planning, contact digitization, and vision-based 3D scanning. CAD-based methods can generate geometry-aware paths based on shoe last models [4,5], but they often fail to accommodate manufacturing tolerances and deviations found in real-world shoes. Contact-based approaches use digitizers and mechanical fixtures to trace upper contours [6], offering simplicity and low cost but relying on manual operation.

A number of studies have explored vision-based trajectory extraction for adhesive application. Some utilize 2D imaging or laser line profile scanning to identify sole contours and spraying paths [7–9], while others employ structured-light or stereo vision to reconstruct the 3D geometry of soles [10–12]. These techniques often work well for relatively flat, rigid surfaces but tend to struggle with complex or flexible upper geometries.

Further work has incorporated laser-based 3D scanning to extract edge or groove features on lasted uppers [13–15], but accuracy tends to degrade when handling soft or less rigid materials. Some systems have integrated structured-light cameras directly onto robotic end-effectors, enabling trajectory acquisition through dynamic scanning [15–17]. However, these implementations are usually constrained to stationary workpieces and do not scale well to conveyor-based production.

More recent developments have explored multi-robot coordination or offline scanning using rotating platforms to construct complete 3D models of the upper for path planning [18–19]. While these systems are technically advanced, they are generally unsuitable for real-time production environments where adaptability and speed are critical. These limitations highlight the need for a more flexible and production-ready solution—one capable of capturing each upper's geometry on the fly, planning adaptive adhesive paths, and executing precise robotic spraying. This study aims to fulfill these requirements by integrating real-time 3D scanning, surface-normal-based path planning, and robotic automation into a cohesive, scalable system.

Beyond technical limitations, the need for automation is further emphasized by the ergonomic and health concerns associated with manual gluing. Workers must handle heavy lasted uppers for extended periods and are exposed to adhesive fumes, increasing the risk of repetitive strain injuries and respiratory issues. Automating this process would reduce occupational hazards while improving consistency and efficiency.

To date, few studies have tackled the end-to-end challenge of customizing adhesive paths for individually shaped lasted uppers, especially considering curvature variation, path orientation, and actual production deployment. To address these challenges, this study proposes a fully integrated 3D vision-guided robotic gluing system for automated adhesive spraying on lasted uppers. The system leverages structured-light 3D scanning, OpenCV and PCL-based point cloud processing, and real-time trajectory generation to customize robotic paths for each shoe. A six-axis robotic arm performs the adhesive spraying while dynamically adjusting orientation of the lasted upper to align the surface normal with the fixed nozzle, ensuring uniform adhesive coverage. In addition, the system includes UV-based fluorescence detection to verify glue application quality.

This research addresses that gap by integrating real-time 3D vision, dynamic path planning, and robotic execution, validated in a production-line scenario. The main contributions of this work are (1) Development of a multi-angle laser scanning module capable of capturing the 3D profile of various lasted upper styles in real time. (2) Design of a vision-based algorithm to determine the bonding line through 3D model alignment with outsole sidewall reference. (3) Integration of a six-axis robotic arm for dynamic path execution based on surface normal vectors. (4) Deployment and validation of the system in a production setting, demonstrating consistent adhesive coverage and repeatability within ±0.5 mm, well below industry tolerances.

This work offers a scalable and intelligent solution to replace manual adhesive application in footwear production lines, improving process stability, safety, and labor efficiency. Unlike prior work, this system has been successfully deployed in a live production line in Hanoi, Vietnam, demonstrating its industrial feasibility and robustness in handling real-world variability without

 doi:10.20944/preprints202504.1336.v1

relying on CAD data or manual path teaching. This research marks a significant advancement toward intelligent and scalable adhesive automation in the footwear industry.

2. Methods for 3D Model Generation

In 3D measurement, the techniques are generally classified into two categories: **contact-based** and **non-contact-based** methods. Non-contact measurement based on computer vision eliminates the need for physical contact with the target object, thereby minimizing the risk of damage. In addition, it offers significantly higher measurement speed compared to traditional contact-based methods. Due to these advantages, the non-contact approach was selected for our application.

2.1. Structured Light

Structured Light is a 3D imaging technology [20] that uses known light patterns (such as stripes, dot grids, or specific shapes) projected onto an object's surface. A camera then captures how these patterns deform when interacting with the object, as shown in Figure 1. By analyzing the deformation of the patterns, the system calculates the depth information of the surface, enabling the creation of a 3D model of the object.

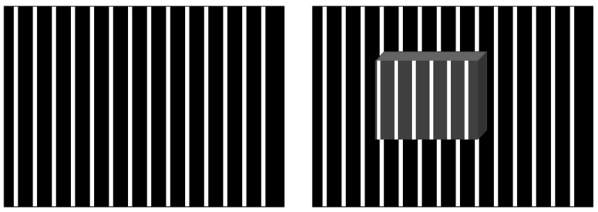

Figure 1. Schematic diagram of structured light principle.

2.2. Laser Triangulation

Laser triangulation [21] is another type of non-contact 3D measurement technique based on geometric principles. It is widely utilized in industrial inspection, machine vision, and automation due to its accuracy and robustness. When a laser beam is projected onto the surface of the target object, it forms a laser line whose position on the surface varies with changes in the object's height. By measuring the position of this line's image on the sensor, the depth information of the object can be calculated.

As illustrated in Figure 2, this study employs a standard geometric configuration in which the laser beam is projected perpendicularly onto the measurement plane of the object (the x–y plane), while the camera observes the resulting laser line at an angle α. Note that as the object's height changes, the magnification of the camera also varies. To deal with this variation, a linear regression analysis and least squares method are used in this study to fit a transformation curve between the laser's pixel position and the actual height values [22]. This transformation curve is then used to infer the surface depth information of the object under test, which will be discussed in detail later.

 doi:10.20944/preprints202504.1336.v1

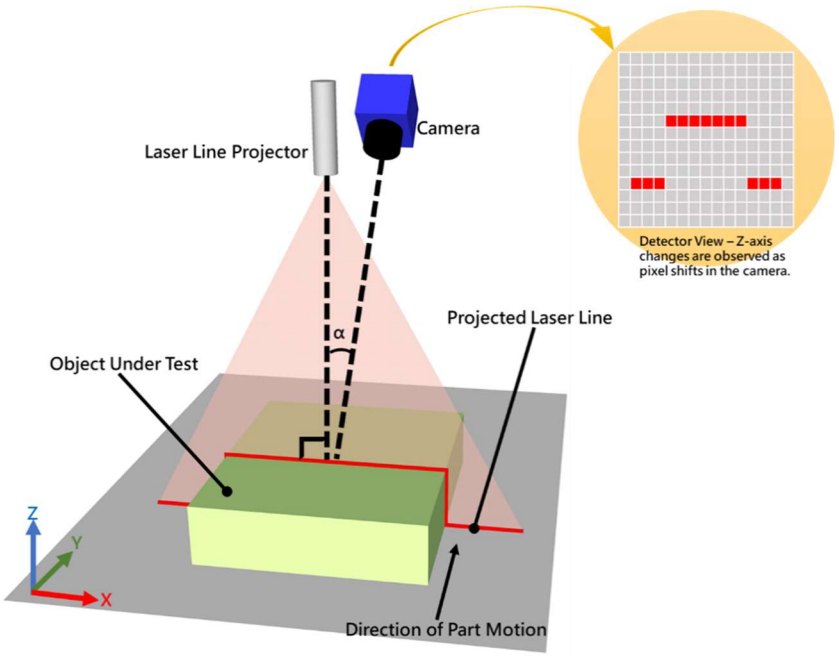

Figure 2. Schematic diagram of laser triangulation measurement.

2.3. Point Cloud

Point Cloud is a collection of three-dimensional data used to represent an object or space. As shown in Figure 3, it is obtained by performing 3D sampling on the surface of an object. Each point contains a set of XYZ coordinates based on the Cartesian Coordinate System. The formation of a point cloud can be achieved using the aforementioned methods, including structured light and laser triangulation. In this study, laser triangulation is employed to capture the depth profile of the shoe upper, which is then reconstructed into a 3D model using the open-source C++ Point Cloud Library (PCL) [23]. The 3D model of the shoe upper will be integrated with that of the outsole to facilitate the planning of the adhesive coating (spraying) path.

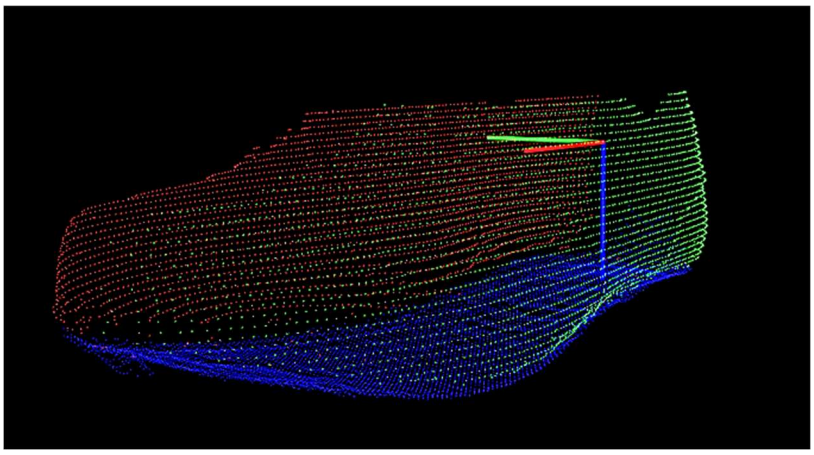

Figure 3. Example of 3D point cloud map.

3. System Hardware Architecture

The hardware architecture of this system includes a laser triangulation based 3D scanning system, four six-axis robotic arms (two for the treatment agent coating and two for water-based adhesive coating), a conveyor system, a lasted upper transfer turntable, three lasted upper transfer mechanism, and several drying ovens. The **lasted upper** refers to the upper part of a shoe after it has been stretched and shaped over a "last" (a foot-shaped mold) during the shoemaking process.

 doi:10.20944/preprints202504.1336.v1

Additionally, the main control computer supervises the entire production line, including the operation of the robotic arms. The overall hardware system architecture is depicted in Figure 4, and the functions of each component are described in the following subsections.

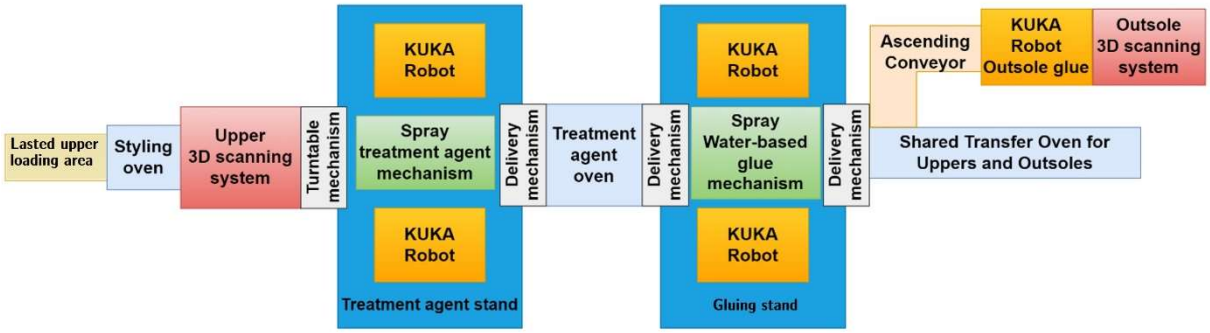

Figure 4. Diagram for system architecture of hardware components

3.1. Loading Area and Oven

As shown in Figure 4, the operator first places the lasted upper onto the conveyor line at the lasted upper loading area. Since the lasted upper has been pre-sprayed with water, it passes through the first (styling) oven during transportation. This oven evaporates the moisture inside the upper, which not only helps shape the upper but also facilitates the treatment agent at the next station to penetrate more effectively into the gaps of the upper fabric.

3.2.3. D Scanning System

In the production line, the transfer of lasted uppers between stations, 3D scanning at the scanning station, and coating at the treatment agent and water glue stations all require the lasted uppers to be clamped for operation. Therefore, a specialized clamping mechanism was designed based on the shape of the shoe last, as shown in Figure 5a. This custom fixture uses cylinder to drive the clamping jaws and position pins for securing the shoe last in place. With this design, the custom clamping mechanism facilitates transfer, scanning, and coating operation. After exiting the first oven, the lasted upper is gripped by a pneumatic gripper (Figure 5b) and transferred to the 3D scanning system. This system is composed of a transfer platform designed for the lasted upper and a distance measurement unit based on laser triangulation.

To reduce costs, the 3D scanning system employs a self-developed laser triangulation technique to capture the geometry of the upper and reconstruct its 3D model. This system is constructed by setting up three laser triangulation systems, each composed of a camera and a line laser, on the two sides and the top of the lasted upper. Three laser beams from different directions form three lines, two of which are parallel, and the third one (top) is perpendicular to both, three laser lines form a common plane, as shown in Figure 6a. The pneumatic gripper holds the lasted upper, and the transfer platform moves it while synchronized signals from the transfer system trigger the camera to capture the laser lines on the upper. Putting these components all together, the overall system implemented is shown in Figure 6b.

 doi:10.20944/preprints202504.1336.v1

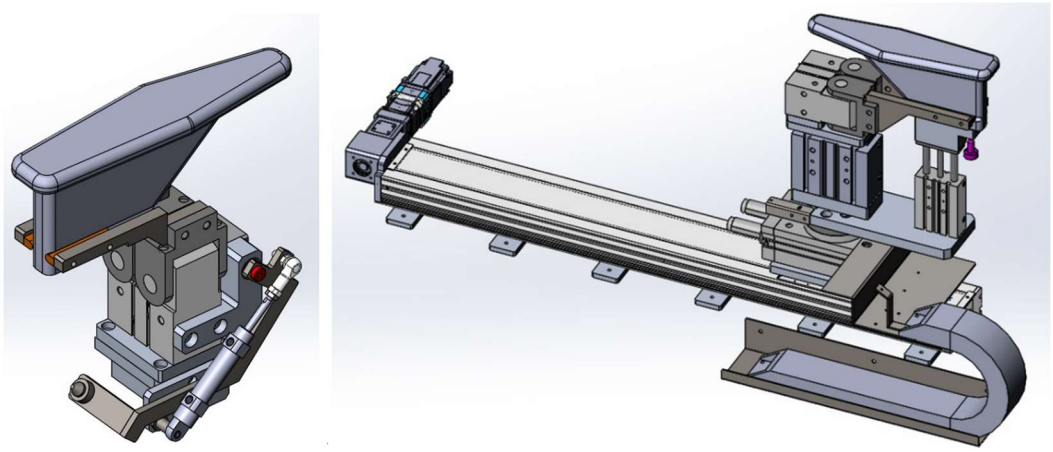

(**a**) (**b**)

Figure 5. (a)3D diagram of pneumatic gripper. (b) 3D diagram of lasted upper transfer platform.

The system simultaneously scans the left and right sides, as well as the bottom of the upper. The data from the three sets of scans are integrated to acquire the complete 3D information of the upper. This enables real-time generation of 3D models for various shoe designs, allowing the system to determine the precise adhesive spray positions and angles tailored to each shoe model.. It ultimately generates a customized spray path for the robotic arm. Once the path is constructed, the rotary table mechanism transfers the lasted upper to the next station for treatment agent coating.

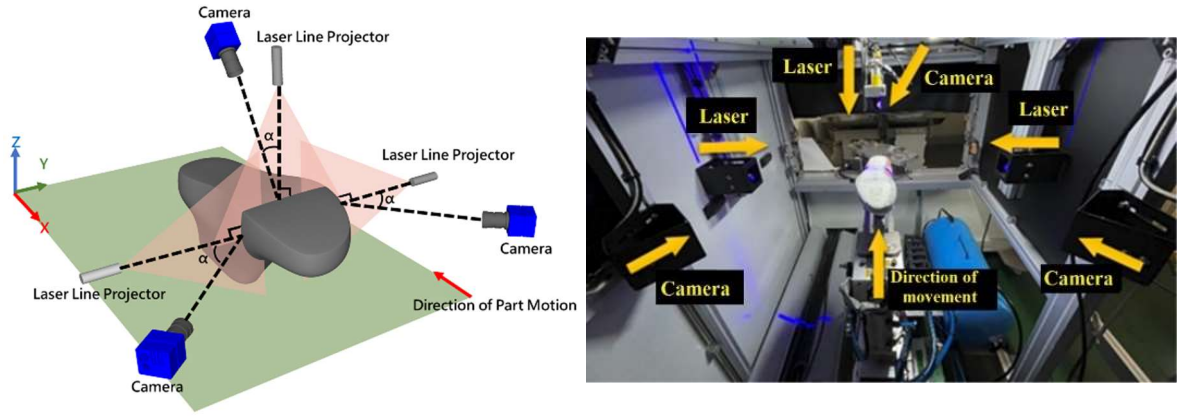

(**a**) (**b**)

Figure 6. (a)Relative position of the three triangulation systems. (b)Implemented 3D scanning system.

3.3. Rotational Mechanism and Transfer Mechanism

A multi-axis transfer device is installed between the 3D scanning station and the treatment agent station. After scanning is completed at the 3D scanning station, the robotic arm at the treatment agent station cannot directly retrieve the shoe last from the gripper at the 3D scanning station. Therefore, a mechanism which has rotation, translation and tilting functions (as shown in Figure 7a) is required to firstly rotate the shoe last and then translate and tilt for the gripper jig on the robotic arm (see Figure 5a) to grip it.

After treatment agent has been applied, another fixture is needed to receive the shoe last detached from the six-axis robotic arm, as shown in Figure 7b. It then tilts down to a level position and a pneumatic clamp would take it back onto the conveyor. These devices will also be used at the adhesive spraying station.

 doi:10.20944/preprints202504.1336.v1

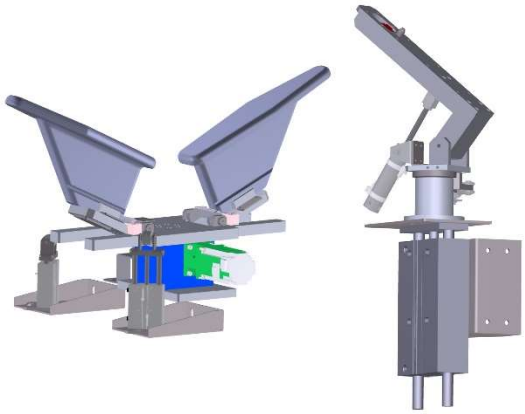

(**a**) (**b**)

Figure 7. (a) A mechanism for clamping, rotating, translating, and tilting. (b) A mechanism for receiving the shoe last from the robotic arm.

3.4. Treatment Agent and Water-Based Adhesive Coating Station

At the treatment agent station, the robotic arm uses a pneumatic gripper to hold the lasted upper and executes the spraying operation along the path generated in the previous stage. To precisely control the coating area, the system adopts a fixed spray gun (Figure 8a) while the robotic arm maneuvers the lasted upper close to the spray baffle for coating, as highlighted within the circle in Figure 8b. In this study, the term *spray baffle* refers to a fixed mechanical structure positioned in front of the spray nozzle. Its primary function is to constrain the adhesive spraying direction, guide the application path, and prevent overspray or adhesive overflow onto unintended regions of the shoe upper. During the spraying process, the robotic arm moves the shoe last close to the spray baffle to ensure proper alignment and uniform adhesive application.

This method differs from the conventional approach of fixing the lasted upper in place and having the robotic arm hold the spray gun for spraying. Although the latter is faster, it is very challenging to achieve precise control over the coating area. Moreover, the lasted upper is usually sprayed while positioned upside down in the latter approach, there is a risk of residual spray agent flowing downward onto the upper surface.

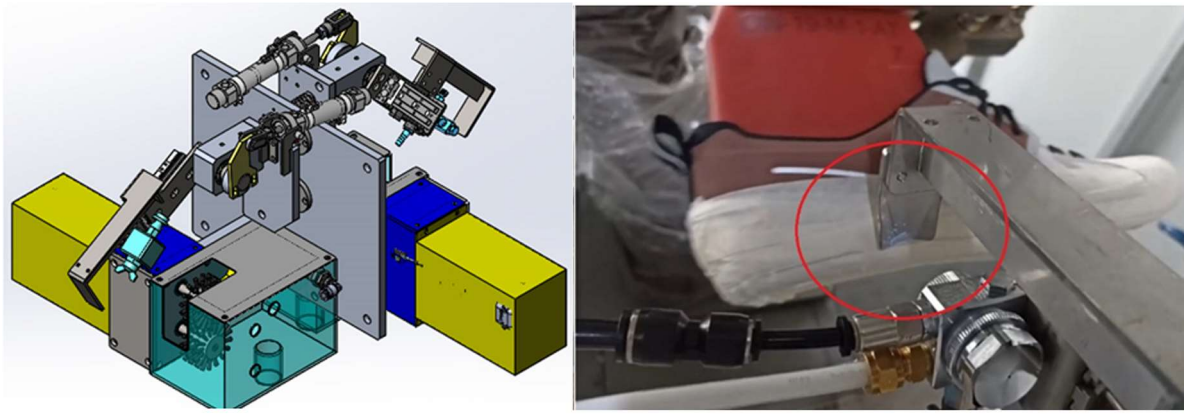

(**a**) (**b**)

Figure 8. 3D diagram of the spraying and cleaning mechanism with integrated spray baffle. (b) Spraying operation in progress near the fixed baffle.

After completing the treatment agent coating, the transfer mechanism returns the lasted upper to the conveyor line, which then delivers it to the second oven for drying. The subsequent water-based adhesive coating station performs the same actions as the treatment agent station. Note that, since the outsole production line applies adhesive at a faster rate than the upper production line, the

 doi:10.20944/preprints202504.1336.v1

treatment agent and adhesive spraying stations for the upper are designed with two parallel lines: one dedicated to processing the right shoe upper and the other to the left, as illustrated in Figure 9.

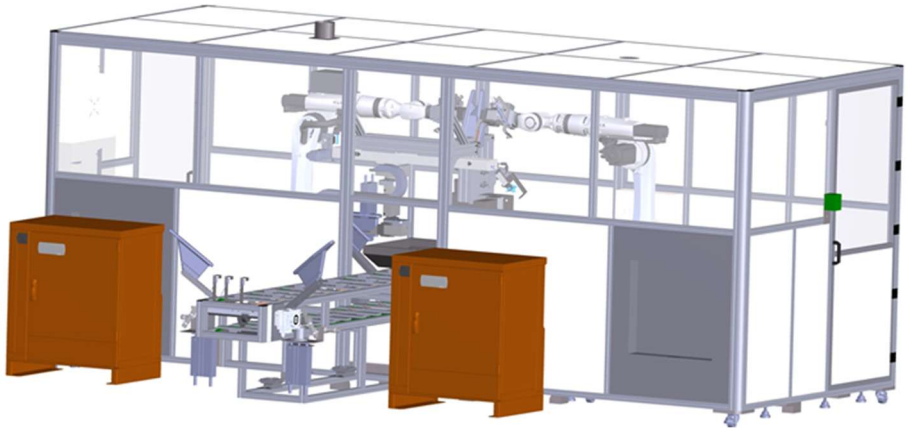

Figure 9. Both robotic arms operate in parallel to spray the left and right lasted uppers.

3.4. Shared Oven and Bonding Area

After completing the adhesive spraying process, the water-based adhesive station transfers the lasted upper into the third-stage oven, which is shared by both the lasted upper and the outsole. In this oven, the outsoles are conveyed along the upper level, while the lasted uppers move along the lower level. At the oven's exit, personnel retrieve both components for bonding, thereby finalizing the entire adhesive application process.

4. Software System

The software system for automated adhesive application on lasted uppers is architected in two parts, each deployed on a separate computer. One computer functions as the main controller, managing the overall production line—including the user interface—and coordinating the robotic arm. The other is an industrial PC dedicated to 3D modeling of the lasted upper and adhesive spray path planning. Communication between the two systems is synchronized via a custom protocol. This paper focuses exclusively on the results of 3D modeling and path planning.

4.1. 3D Modeling of the Lasted Upper

In the 3D scanning system described in Section 3.2, three cameras are employed to acquire laser line images from the left, right, and top perspectives. Each image capture yields a single laser line representing the surface height profile at a specific location. To overcome this limitation, the system integrates a shoe last transfer platform (Figure 5b) capable of grasping and repositioning the shoe last. This enables the cameras to continuously acquire sequential images from different positions. By aggregating the height data captured by the three scanning modules, individual 2.5D depth maps of the lasted upper are generated from each respective view. These depth maps are then merged to reconstruct a unified 2.5D representation of the lasted upper's surface geometry.

4.1.1. Image Acquisition

The scanning process begins when the main control system instructs the scanning module to initiate image acquisition. The shoe last transfer platform then clamps and moves the lasted upper, during which a trigger generation module synchronizes the camera captures with the platform's motion. Upon reaching the end position, the system signals the scanning module to complete the process.

 doi:10.20944/preprints202504.1336.v1

To accurately define the adhesive application areas—located on the bottom and the curved sidewalls of the lasted upper—three scanning setups are employed, as shown in Figure 5, to capture views from the left, right, and bottom. This configuration enables the system to generate a complete 2.5D model of the lasted upper in a single scanning cycle, covering both the side and bottom surfaces. A sample image captured during this process is shown in Figure 10a.

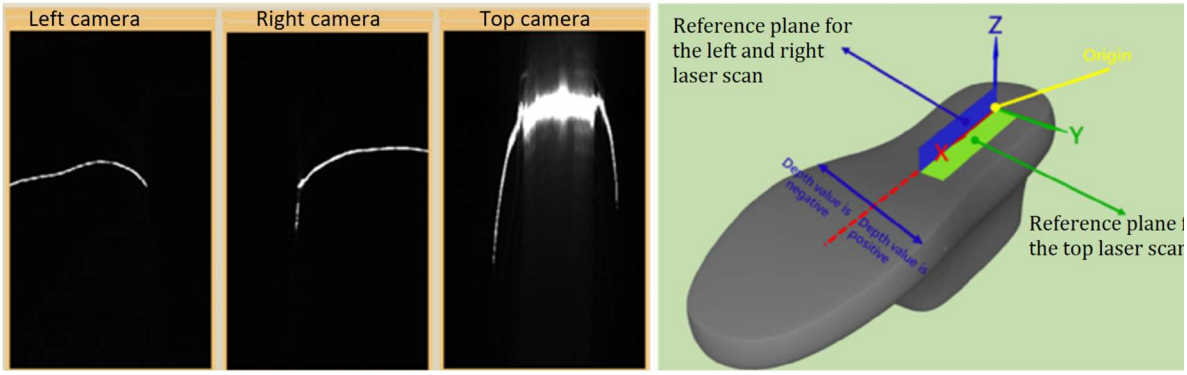

(**a**) (**b**)

Figure 10. (a) Three-sided laser imaging results in one shot. (b) Definition of the reference plane of shoe upper.

When constructing a 3D model using the three laser triangulation systems, a common reference plane must be established to unify the height measurements. As shown in Figure 10b, the first reference plane—defined as the X-Z plane with a height value of 0 mm—is located between the left and right laser setups. Height values from the left and right scans are assigned negative and positive signs according to the direction of the Y-axis in the figure. Additionally, a second reference plane, the X-Y plane, is defined perpendicular to the left–right baseline to serve as the 0 mm reference for the top-view laser. This dual-plane calibration allows all three systems to perform height measurements within a unified coordinate framework.

After establishing the reference planes, the laser line image data must be converted into height information using geometric triangulation principles. This process involves addressing two key challenges. The first is that the laser line images lack sufficient resolution due to the thickness of the laser stripe. The second is that the displacement of the laser line is not linearly proportional to the actual height values. The following sections detail the methods employed to overcome these issues.

4.1.2. Precise Laser Line Localization

When the laser line is projected onto the lasted upper, it is necessary to adjust the camera's aperture and exposure time to capture a sufficiently clear laser image while maintaining compatibility with the required production line speed. As shown in Figure 11a, although the laser image appears clear, the laser stripe remains too thick to enable precise localization. To improve accuracy, adaptive thresholding is first applied for binarization, followed by morphological closing and contour tracing techniques [24]. These image processing steps extract the contour edge points of the laser stripe, as illustrated in Figure 11b,c.

Subsequently, based on the extracted upper and lower contour edge points, the laser stripe's centerline is computed by determining the midpoint between the two edges in each image row. This approach assumes a symmetrical laser intensity distribution, allowing the centerline to represent the geometric center of the stripe's visible width. The resulting centerline provides a subpixel-accurate estimation of the stripe position and serves as the basis for calculating displacement values, as illustrated in Figure 11(d). In cases where the lasted upper exhibits complex textures or surface patterns, small gaps may appear along the extracted contours. As these discontinuities are typically minor, they can be effectively filled using linear interpolation.

Preprints.org (www.preprints.org) | NOT PEER-REVIEWED | Posted: 16 April 2025 doi:10.20944/preprints202504.1336.v1

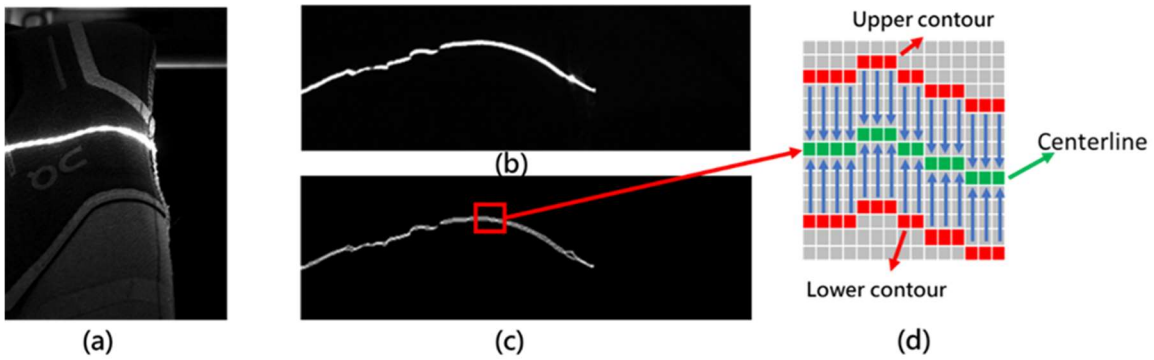

Figure 11. (a)Original laser image. (b)Binarization and closing. (c)Contour tracing. (d) Centerline extraction.

4.1.3. Transformation Curve for Displacement to Height Conversion

Through the aforementioned thinning process, a precise centerline of the laser stripe is obtained, representing the pixel displacement relative to a defined reference. The next step involves converting this displacement into an actual height value using geometric triangulation. However, due to the nonlinear projection geometry inherent in laser triangulation systems, the horizontal displacement of the laser stripe is not linearly proportional to the corresponding surface height.

To address this, a calibration procedure is conducted using 650-series industrial-grade gauge blocks manufactured by the U.S. precision tooling company Griffin, as shown in Figure 12a. These blocks serve as reference objects to establish the mapping between pixel displacement and physical height. For each gauge block of known height, the corresponding laser stripe position is recorded. As illustrated in Figure 12b, the imaging position of the laser stripe shifts with height—higher gauge blocks result in lower y-axis coordinates in the image. This inverse relationship is later modeled using polynomial regression to form the basis of the height-displacement conversion function.

Once the calibration curve is established, it is applied to the centerline data obtained from the lasted upper to compute the relative height of each point with respect to the reference plane.

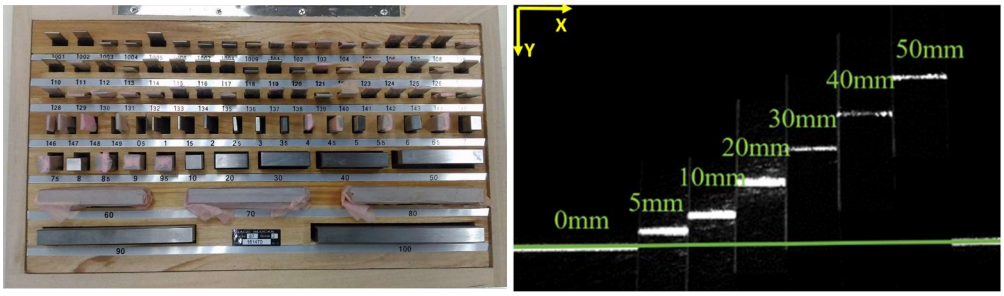

Figure 12. (a) Industrial-grade gauge blocks. (b) Laser line displacement for gauges with varying block heights.

During the calibration process, images can only be acquired using a limited number of gauge blocks with fixed heights. However, the lasted upper surface features continuous height variations. To address this, interpolation is employed to establish a conversion function between displacement and height based on a finite set of reference data points. Experimental results confirm that the relationship between displacement and height is nonlinear. Accordingly, the least squares method is applied to fit a quadratic polynomial to the measured data, providing a continuous mapping from pixel displacement to real-world height.

In the experiment, multiple pairs of two-dimensional data (x_i, y_i) are collected using gauge blocks of known heights, where x_i denotes the physical height and y_i represents the corresponding pixel displacement observed in the image. These data points are then used to perform curve fitting, resulting in a second-order polynomial as shown in Equation (1). The coefficients a, b, and c are

 doi:10.20944/preprints202504.1336.v1

determined via the least squares method and characterize the displacement-to-height mapping function.

$$y = ax^2 + bx + c \tag{1}$$

The objective is to minimize the sum of squared errors between the measured data and the quadratic curve, as expressed in Equation (2).

$$E = \sum_{i=1}^{n} \left(y_i - \left(ax_i^2 + bx_i + c\right)\right)^2 \tag{2}$$

Express the aforementioned quadratic curve in matrix form:

$$\mathbf{E} = \mathbf{Y} - \mathbf{X} \cdot \boldsymbol{\beta}$$

where the observation vector $\mathbf{Y}$ represent the measured displacement data, the design matrix $\mathbf{X}$ represent the polynomial expansion of the input height values, and the parameter vector $\boldsymbol{\beta}$ denote the coefficients of the quadratic function to be estimated, they are:

$$\mathbf{Y} = \begin{bmatrix} y_1 \\ y_2 \\ \vdots \\ y_n \end{bmatrix}, \ \mathbf{X} = \begin{bmatrix} x_1^2 & x_1 & 1 \\ x_2^2 & x_2 & 1 \\ \vdots & \vdots & \vdots \\ x_n^2 & x_n & 1 \end{bmatrix}, \ \boldsymbol{\beta} = \begin{bmatrix} a \\ b \\ c \end{bmatrix} \tag{3}$$

Using the least squares method, the objective is to minimize the sum of squared residuals, i.e., $\|\mathbf{X}\boldsymbol{\beta} - \mathbf{Y}\|^2$. The optimal solution provided by the least squares method can be obtained by solving the normal equation $\mathbf{X}^{\mathrm{T}}\mathbf{X}\boldsymbol{\beta} = \mathbf{X}^{\mathrm{T}}\mathbf{Y}$. Compute $\mathbf{X}^{\mathrm{T}}\mathbf{X}$ and $\mathbf{X}^{\mathrm{T}}\mathbf{Y}$:

$$\mathbf{X}^{\mathrm{T}}\mathbf{X} = \begin{bmatrix} \sum x_i^4 & \sum x_i^3 & \sum x_i^2 \\ \sum x_i^3 & \sum x_i^2 & \sum x_i \\ \sum x_i^2 & \sum x_i & n \end{bmatrix}, \ \mathbf{X}^{\mathrm{T}}\mathbf{Y} = \begin{bmatrix} \sum x_i^2 y_i \\ \sum x_i y_i \\ \sum y_i \end{bmatrix} \tag{4}$$

By solving $\boldsymbol{\beta} = (\mathbf{X}^{\mathrm{T}}\mathbf{X})^{-1}\mathbf{X}^{\mathrm{T}}\mathbf{Y}$, the values of $\boldsymbol{\beta}$ are obtained, where $\boldsymbol{\beta} = [a \quad b \quad c]^T$. The transformation curves for the right, left, and top scanning systems, derived from the experimental data, are presented in Figure 13.

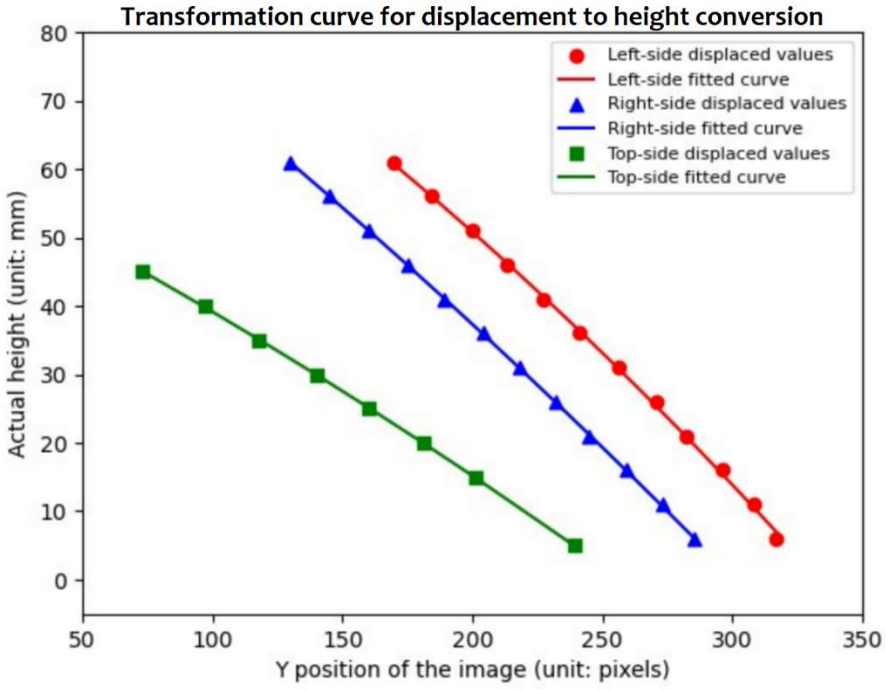

Figure 13. Transformation curve fitted using the least squares method.

 doi:10.20944/preprints202504.1336.v1

4.1.4. From Depth Image to 3D Model

Using individual laser ranging systems, the height values obtained from the transformation curves of each laser stripe are combined to construct a 2.5D depth image of the lasted upper. Figure 14 presents the 2.5D depth images of the left side, right side, and bottom of the lasted upper, respectively. In each image, the grayscale value of a pixel represents its corresponding height, where lower grayscale values indicate lower surface elevations, and higher grayscale values correspond to greater heights.

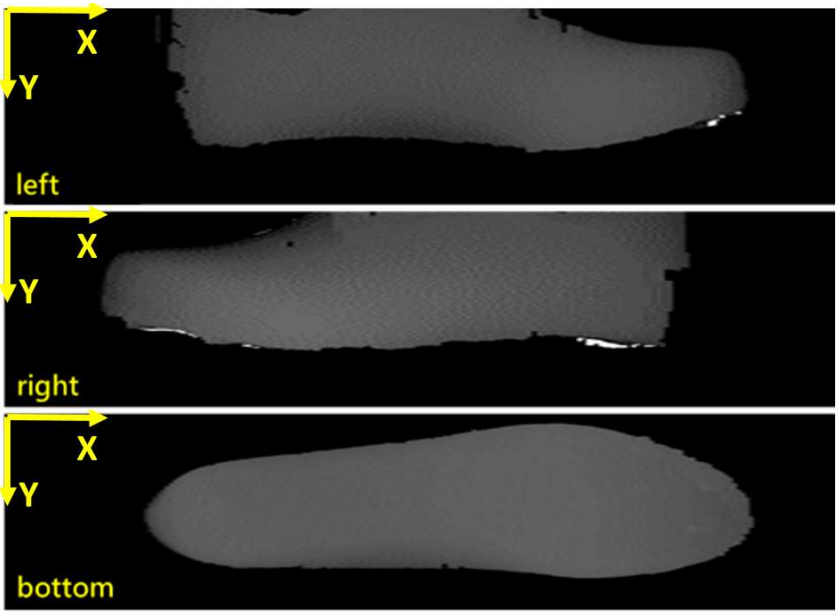

Figure 14. 2.5D depth images generated from individual scanning views: (Top) left side, (Middle) right side, and (Bottom) top view of the lasted upper. Grayscale values represent relative height.

In the three 2.5D depth images, the grayscale values representing height have already been converted to physical units in millimeters. However, the X and Y directions, as indicated in the top-left corner of each image, are still expressed in pixel units. To obtain accurate physical dimensions, the pixel values in the XY directions must be multiplied by the corresponding pixel-to-millimeter conversion factors. This transformation is essential for reconstructing a geometrically accurate 3D model with real-world units (mm), and the process is discussed in the following section.

In the depth images shown in Figure 14, the X-coordinate in each image corresponds to the index of the x-th laser scan. As the lasted upper is moved by a transfer platform at a known constant speed v (mm/s), and the camera is triggered at a fixed interval t (s) by the signal generation module, the actual scanning interval can be calculated as vt (mm) per trigger. Therefore, by multiplying this interval distance by the X-coordinate index x, the X-axis pixel position can be converted into a physical length in millimeters, enabling accurate spatial representation of the shoe surface.

In contrast to the X-axis, the unit conversion along the Y-axis is more complex. While the X-axis directly corresponds to the scan sequence and the known movement speed of the transfer platform, the physical length represented by each pixel in the Y-axis varies with height. This variation arises from the camera's perspective geometry and optical properties, which cause nonlinear scale changes at different heights. As the laser stripe shifts vertically due to height differences, the pixel spacing in the Y-axis changes accordingly. As illustrated in Figure 15, when a gauge block with a known width of 9 mm is placed at different heights, the same physical width appears as different pixel lengths in the captured images. This observation confirms that the pixel-to-millimeter conversion factor (mm/pixel) along the Y-axis is height-dependent and must be adjusted accordingly during reconstruction.

 doi:10.20944/preprints202504.1336.v1

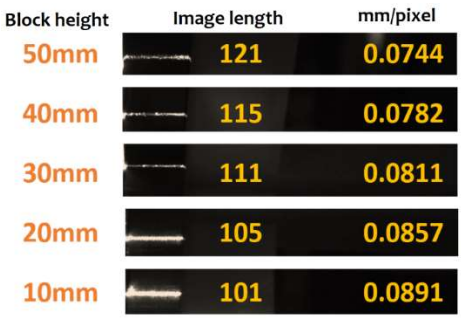

Figure 15. Variations of pixel resolution at different height.

To address this issue, a variable Y-axis scaling function is established using calibration data collected from all three scanning systems. Similar to the previous steps, images of reference objects—such as gauge blocks—at various known heights are captured, and the corresponding pixel-to-millimeter ratios are computed. Based on this dataset, three interpolation functions are derived for the left, right, and bottom views of the lasted upper, respectively, enabling dynamic adjustment of the Y-axis scaling factor according to the local height. Once the unit conversions along both the X and Y axes are completed, the three sets of 2.5D depth data obtained from laser scanning can be transformed into 3D point cloud data. These point clouds are subsequently used to reconstruct a complete 3D model of the lasted upper.

As shown in Figure 16, the point cloud model is constructed by merging three sets of point cloud data captured from the left, right, and bottom views of the lasted upper. Following model construction, the coordinate system is transformed to align with that of the robotic arm. This alignment is accomplished by applying a coordinate transformation matrix, which will be described in a subsequent section. Through this transformation, the 3D point cloud is accurately mapped into the robot's working space, enabling precise motion planning and adhesive path generation. The resulting merged point cloud provides an accurate geometric representation of the lasted upper surface, serving as the foundation for downstream adhesive application.

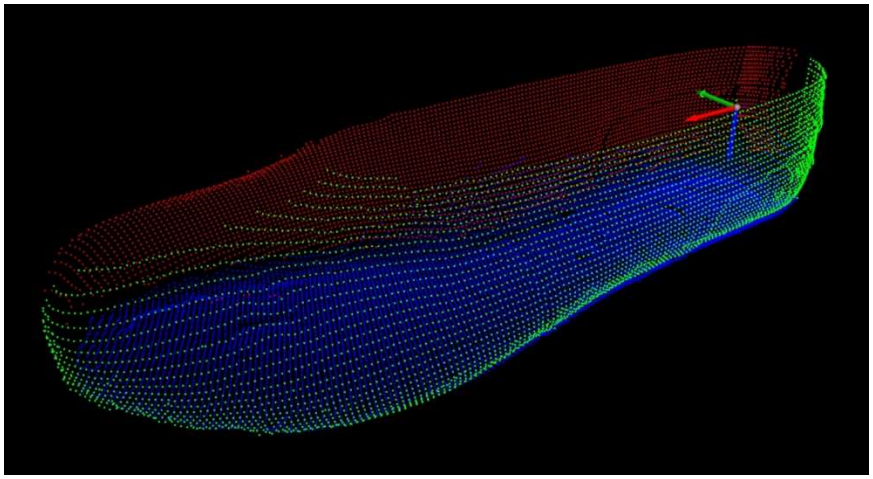

Figure 16. Merged 3D point cloud of the lasted upper, constructed from three scanning views and aligned with the robotic coordinate system. Color coding: green – left side; red – right side; blue – bottom.

4.2. Path Planning

Once the 3D point cloud of the lasted upper is acquired, it can be used in conjunction with the corresponding 3D outsole model to plan the adhesive application path. In the shoe manufacturing process, the lasted upper undergoes manual stitching and lasting, resulting in greater geometric variation compared to the outsole. Therefore, to ensure precise bonding, each lasted upper must be

 doi:10.20944/preprints202504.1336.v1

individually scanned in 3D prior to adhesive application. In contrast, outsole variations are minimal, as their dimensions remain highly consistent throughout production. As such, 3D models of all available outsole sizes—both left and right—can be pre-scanned and stored in a database. These pre-scanned outsole models are then utilized during path planning for each upper, enabling accurate adhesive application regardless of individual shape differences.

The adhesive path planning procedure involves the following steps:

1. Identifying the foot orientation (left or right) and size of the lasted upper.
2. Aligning the adhesive line of the lasted upper with the corresponding height profile of the outsole.
3. Extracting normal vectors along the adhesive line to guide precise robot motion and ensure proper spray direction.

4.2.1. Identifying the Upper's Foot Orientation (Left or Right) and Size

As mentioned earlier, the 3D point cloud model of the lasted upper is generated using three scanning systems positioned at different orientations. The laser scanning system mounted above, which captures the bottom of the lasted upper, serves three main functions. First, it enables the seamless integration of laser data from the top region with those from the left and right scanning systems, thereby supporting the reconstruction of a complete 3D model of the side surfaces. Second, it provides the pixel-to-millimeter conversion factor based on variations in the surface height, ensuring an accurate 3D model of the bottom of the lasted upper. These two functions have already been utilized in the previous section.

The third function is to use the depth image captured from the bottom of the lasted upper to determine its size and identify whether it belongs to the left or right foot in real time. As shown in Figure 17, for a given depth image, the width of the lasted upper L1, is measured at the 7/10 position of the model. By connecting its center position P1 to the toe tip P2, the slope of vector $\overrightarrow{P_1P_2}$ is found to be positive, then it is a left- foot upper. Conversely, if the slope is negative, the lasted upper is identified as a right foot. Additionally, by measuring the distance from the toe tip to the heel, the shoe size can be determined. Based on the estimated size and foot orientation, the corresponding outsole 3D model is retrieved from the database. The 3D model of the lasted upper is then aligned and merged with its matched outsole model. This combined geometry serves as the basis for generating the adhesive dispensing path.

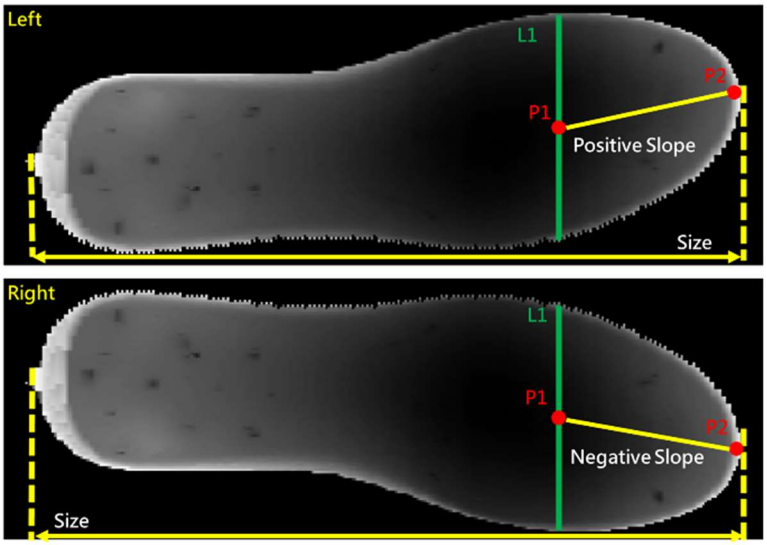

Figure 17. Bottom view depth image of the lasted upper for determining size and foot orientation.

4.2.2. Alignment of the Adhesive Line with the Outsole Height Profile

 doi:10.20944/preprints202504.1336.v1

In traditional manual adhesive application for the lasted upper, the outsole is first temporarily fitted onto the upper, and a bonding line is manually marked around the upper to indicate the height of the outsole's sidewall. After removing the outsole, adhesive is applied to the region below this bonding line, as illustrated in Figure 18.

In the automated process, a similar approach is adopted. First, the bonding line must be identified on the 3D model of the lasted upper. This is accomplished by aligning the 3D point cloud of the lasted upper with its corresponding outsole model. Once the outsole's sidewall is properly registered with the upper in 3D space, the bonding height is extracted from the outsole geometry and projected onto the upper surface, thereby defining the bonding line. Based on this bonding line, an adhesive line is then generated to guide the robotic arm's spraying path. This ensures that adhesive is applied only within the intended bonding region, replicating the precision of manual processes while enabling automation.

Figure 18. Schematic diagram showing the outsole and its corresponding bonding line on the lasted upper.

Since the 3D models of the outsole and the shoe upper are acquired using different scanning devices, they must first be registered within a common coordinate system. This alignment is critical to ensure that the outsole's sidewall can be accurately used to define the bonding line on the upper surface. As illustrated in Figure 19, subfigure (a) shows the depth map of the shoe upper from both sides, while subfigure (b) presents the depth map of the outsole. It is evident that a translational and rotational offset exists between the two models due to differences in their respective scanning coordinate systems. Without proper alignment, directly overlaying the outsole onto the upper results in the misalignment shown in subfigure (c), where the geometries fail to correspond accurately.

To resolve the XY-coordinate offset between the shoe upper and outsole models, a set of key reference points is used to estimate the translational displacement. Specifically, two center points—p1and p2—are extracted from the shoe upper point cloud at one-quarter and three-quarters of its total length, respectively, by averaging the coordinates across its width at those locations. Similarly, two corresponding points—p3 and p4—are selected from the outsole model using the same longitudinal proportions and lateral centering method. These four points form two longitudinal reference lines, one on the upper and one on the outsole, which are then used to compute the required XY translation vector for alignment.

 doi:10.20944/preprints202504.1336.v1

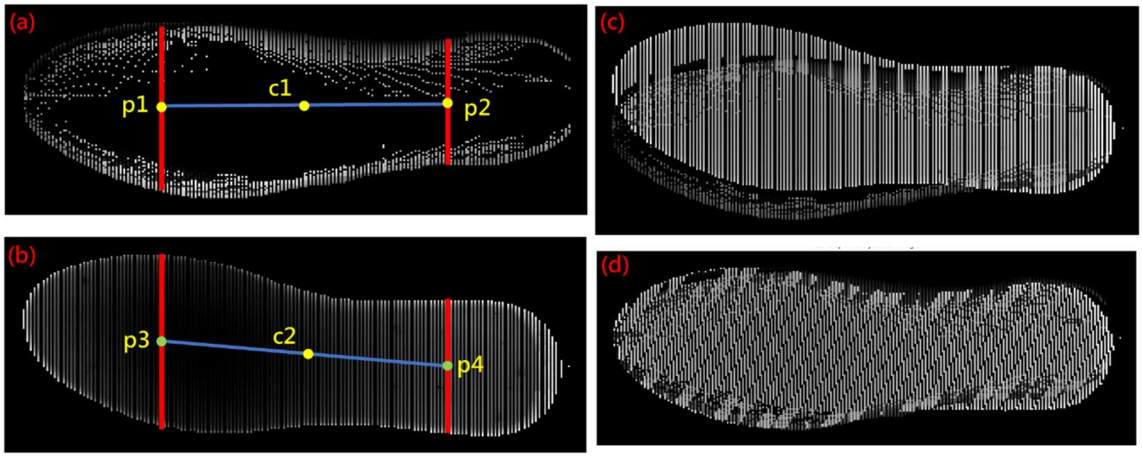

Figure 19. Depth map-based alignment of the lasted upper and outsole.

Next, the slope $m1$ and center coordinate $c1$ of the line connecting points p1 and p2 on the shoe upper are computed, along with the slope $m2$ and center coordinate $c2$ of the line connecting points p3 and p4 on the outsole model. Based on these values, the translational offset **D** of the outsole relative to the shoe upper in the XY plane, as well as the rotation angle θ, can be determined using the equations provided below.

$$c1 = \left(\frac{p1_x + p2_x}{2}, \frac{p1_y + p2_y}{2}\right), c2 = \left(\frac{p3_x + p4_x}{2}, \frac{p3_y + p4_y}{2}\right) \quad (5)$$

$$D_x = c2_x - c1_x \ , \ D_y = c2_y - c1_y \quad (6)$$

$$m1 = \frac{p2_y - p1_y}{p2_x - p1_x}, m2 = \frac{p4_y - p3_y}{p4_x - p3_x}, \theta = tan^{-1}(m2) - tan^{-1}(m1) \quad (7)$$

Using the computed rotation angle and translation vector, the XY coordinates of the outsole's 3D model are corrected to align with those of the shoe upper. Figure 19(d) shows the depth map after applying this alignment, illustrating the successful registration of the outsole with the upper model. Following the XY alignment, a spraying boundary line is defined on the upper surface based on the height of the outsole's sidewall. This boundary, which varies along the contour of the upper, serves as the bonding line for adhesive path generation.

4.2.3. Surface Normal Extraction for Orientation Control in Adhesive Path Generation

To enable the robotic arm to execute adhesive spraying along the defined path after gripping the lasted upper, the path data must include not only the spatial coordinates (X,Y,Z), but also the angular information required to define the spraying orientation at each point. This orientation information is derived from the constructed 3D point cloud of the lasted upper. For each point along the spraying path, the corresponding surface normal vector is computed and used to determine the required spraying direction.

As illustrated in Figure 20, the generated path is shown along with its associated direction vectors. These surface normal vectors are extracted along the bonding line to ensure that, during spraying, the surface of the lasted upper remains perpendicular to the fixed nozzle. The robotic arm then adjusts the orientation of the upper at each path point by calculating Euler angles that align the local surface normal with the nozzle direction.

 doi:10.20944/preprints202504.1336.v1

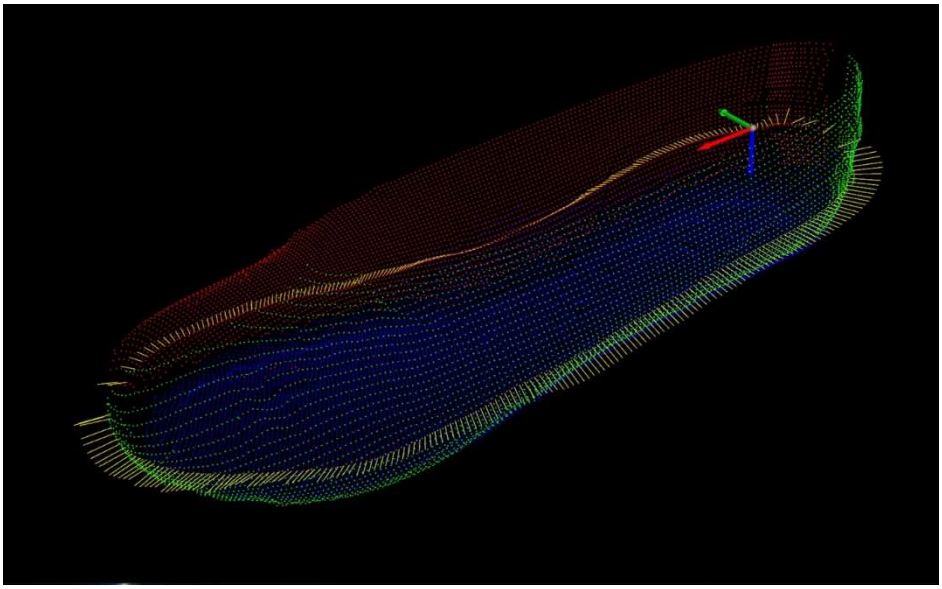

Figure 20. 3D point cloud of the lasted upper with computed surface normal vectors. Yellow lines represent the surface normals along the generated adhesive spraying path.

4.3. Coordinate Transformation from Scanning Frame to External Work Coordinate System

To accurately execute the spraying path derived from the scanned 3D model of the lasted upper, a two-stage coordinate transformation is required. The original path, defined in the scanning coordinate frame, must first be converted to the robotic tool coordinate system. Subsequently, it must be further transformed into the external work coordinate system, whose origin is located at the center of the spray baffle. The following subsections describe these two transformation processes in detail.

4.3.1. Transformation from Scanning Frame to Tool Coordinate System

The spraying path data derived for the lasted upper is initially defined in the coordinate system established by the three-sided laser scanning system described in Section 4.1.1. However, for practical robotic execution, this coordinate system must be transformed into the tool coordinate system of the robotic arm.

In this study, the 3D scanning system and the robotic arm are located in physically separate environments, making it infeasible to directly acquire common reference points in both coordinate systems for conventional calibration. To overcome this limitation, a portable calibration fixture with known geometric features is employed as an intermediate reference object. The fixture is first placed within the scanning system's field of view, and its pose is recorded relative to the scanning coordinate system. It is then transferred to the robotic workspace, where its spatial orientation is identified using the robot's vision system. By capturing the pose of the same fixture in both environments, a transformation matrix—comprising rotation and translation components—is computed to convert the spraying path data from the **scanning coordinate system** into the **robotic tool coordinate system.** This coordinate transformation enables the robotic arm to accurately follow the adhesive spraying path generated from the pre-scanned 3D model of the lasted upper.

In this system, the bottom of the shoe last—gripped by the robotic arm's end-effector—is defined as the tool coordinate system. The origin of this frame, also referred to as the tool center point (TCP), is set at a small circular hole located at the heel of the shoe last. The axes of the tool coordinate system are defined as follows: the Z-axis points outward and normal to the bottom surface of the shoe last; the X-axis points from the heel to the toe along the longitudinal direction of the shoe last; and the Y-axis is determined by the right-hand rule to complete the orthonormal basis.

Preprints.org (www.preprints.org) | NOT PEER-REVIEWED | Posted: 16 April 2025 doi:10.20944/preprints202504.1336.v1

4.3.2. Transformation from Tool Coordinate System to External Work Coordinate System

During operation, the robotic arm holds the shoe last and moves it toward a fixed spray gun. Guided by the spraying path generated by the scanning system, the arm maneuvers the shoe last such that the adhesive application area closely aligns with the spray baffle, allowing the fixed spray head to accurately apply treatment or adhesive onto the upper surface. To achieve this, the spraying path—initially defined relative to the tool coordinate system—must be converted into the external work coordinate system, whose origin is located at the center of the spray baffle. This final coordinate transformation ensures that the robotic arm can move the shoe last precisely along the pre-defined path relative to the fixed spraying apparatus.

To accurately execute the adhesive spraying path relative to the fixed spray baffle, the spraying trajectory—originally defined in the tool coordinate system (T)—must be transformed into the external work coordinate system (W). This transformation requires a sequential application of two homogeneous transformation matrices:

$\boldsymbol{M}_T^B = \begin{bmatrix} R_T & P_T \\ 0 & 1 \end{bmatrix}$ is the transformation from the tool frame (end-effector) to the robot base coordinate system.

$\boldsymbol{M}_B^W = \begin{bmatrix} R_W & P_W \\ 0 & 1 \end{bmatrix}$ the transformation from the robot base to the external work coordinate system, whose origin is set at the center of the spray baffle.

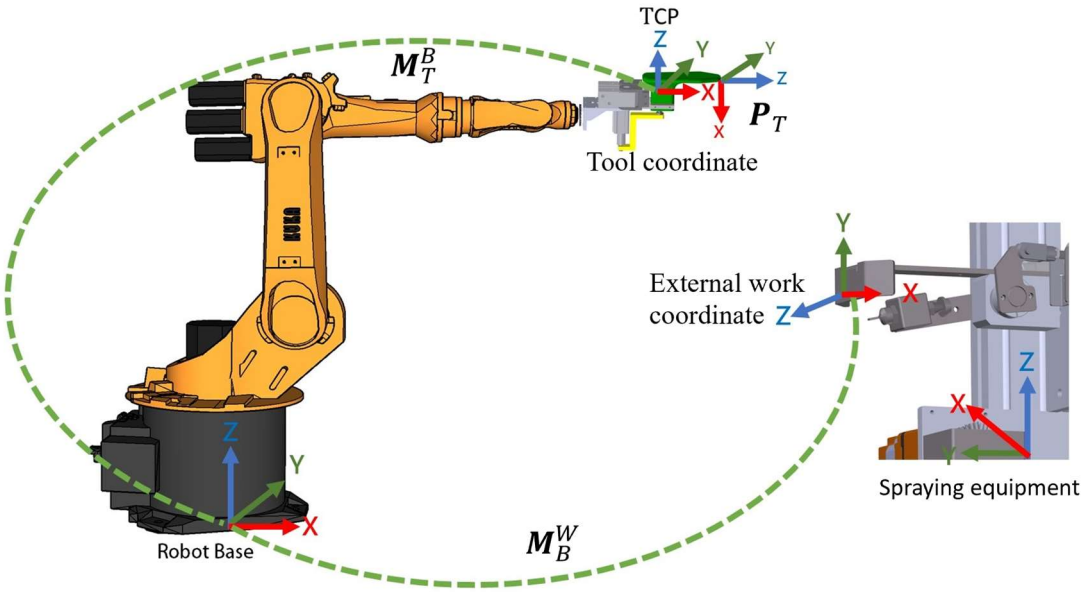

$\boldsymbol{M}_T^B$: Transformation matrix from the tool coordinate system to the robot base.

$\boldsymbol{M}_B^W$: Transformation matrix from the robot base to the external work coordinate system.

Figure 21. Coordinate frame transformation chain from tool to external work coordinate.

The overall transformation from the tool frame to the work frame is given by:

$$\boldsymbol{P}_W = \boldsymbol{M}_B^W \cdot \boldsymbol{M}_T^B \cdot \boldsymbol{P}_T \tag{8}$$

where $\boldsymbol{P}_T = [\mathcal{X}_T, \mathcal{Y}_T, \mathcal{Z}_T, 1]^{\mathrm{T}}$ represents point on the spraying path in the tool coordinate system.

The matrix $\boldsymbol{M}_T^B$ is dynamically provided by the robot controller through its forward kinematics module based on the current joint states. Meanwhile, $\boldsymbol{M}_B^W$ is established via a one-time calibration process by positioning the tool center point (TCP) at known locations on the spray baffle and recording their corresponding base frame coordinates.

As illustrated in Figure 21, this transformation chain enables the robot to convert spraying positions defined relative to the lasted upper (held by the TCP) into precise poses relative to the

 doi:10.20944/preprints202504.1336.v1

external environment. It ensures that the nozzle aligns accurately with the bonding line on the upper surface during adhesive application.

4.4. Pose Calculation Based on Normal Vectors

Each point on the spraying path has an associated normal vector $\boldsymbol{N}_W$ that defines the spraying direction in the external work coordinate system The robotic arm performs the spraying operation along the path defined on the surface of the lasted upper, while the fixed spray tool must remain aligned with the surface normals to ensure uniform adhesive coverage.

The pose of the robotic arm at each path point is typically represented by a combination of position and orientation, where the position is already defined by the transformed path points. The orientation is computed based on the local surface normal vector and the tangent vector along the path. To achieve this, the normal vector and tangent vector are combined to construct a local orthonormal frame, which is then converted into ZYX Euler angles to represent the desired orientation. These Euler angles are used as inputs to the robot controller to achieve accurate pose execution. The computational steps for determining the Euler angles are as follows:

Let $\boldsymbol{P}_i$ represents one of the path points in $\boldsymbol{P}_W(\mathcal{X},\mathcal{Y},\mathcal{Z})$ with associated normal vector $\boldsymbol{\mathcal{N}}_i$, and $\boldsymbol{P}_{i+1}$ is its next path point.

1. Calculation of the tangent vector $\boldsymbol{T}$: It represents the direction of the robotic arm's motion path

$$\boldsymbol{T} = \frac{\boldsymbol{P}_i - \boldsymbol{P}_{i+1}}{\|\boldsymbol{P}_i - \boldsymbol{P}_{i+1}\|} \tag{9}$$

2. Vector $\boldsymbol{T}$ must satisfy the condition of being perpendicular to the normal vector $\boldsymbol{T} \cdot \boldsymbol{\mathcal{N}}_i = 0$. To ensure the system meets this orthogonality condition, we apply the Gram-Schmidt orthogonalization method to adjust the normal vector as follows:

$$\boldsymbol{\mathcal{N}}_i^{'} = \frac{\boldsymbol{\mathcal{N}}_i - (\boldsymbol{\mathcal{N}}_i \cdot \boldsymbol{T})\boldsymbol{T}}{\|\boldsymbol{\mathcal{N}}_i - (\boldsymbol{\mathcal{N}}_i \cdot \boldsymbol{T})\boldsymbol{T}\|} \tag{10}$$

Then, orthogonality condition $\boldsymbol{T} \cdot \boldsymbol{\mathcal{N}}_i' = 0$ now can always be satisfied.

3. Calculation of the binormal vector $\boldsymbol{B}$:

$$\boldsymbol{B} = \boldsymbol{T} \times \boldsymbol{\mathcal{N}}_i^{'} \tag{11}$$

4. Formulate the rotation matrix $\boldsymbol{\mathcal{R}}$: The orthogonal vectors $\boldsymbol{T}$, $\boldsymbol{B}$, $\boldsymbol{\mathcal{N}}_i'$ serve as the basis for describing the robotic arm's rotational orientation.

$$\boldsymbol{\mathcal{R}} = \begin{bmatrix} T_x & B_x & \mathcal{N}_{ix}^{'} \\ T_y & B_y & \mathcal{N}_{iy}^{'} \\ T_z & B_z & \mathcal{N}_{iz}^{'} \end{bmatrix} \tag{12}$$

5. Derive the ZYX-sequence Euler angles from the rotation matrix $\boldsymbol{\mathcal{R}}$:

$$roll = arctan2\left(T_y, T_x\right) \tag{13}$$

$$pitch = arctan2\left(-T_z, \sqrt{B_z^2 + \mathcal{N}_{iz}^{'2}}\right) \tag{14}$$

$$yaw = arctan2\left(B_z, \mathcal{N}_{iz}^{'}\right) \tag{15}$$

After converting the surface normal vector at each point on the spraying path into ZYX Euler angles, the resulting position $\boldsymbol{P}_W$ and orientation can be transmitted to the robotic arm for execution. Each computed spraying point is formatted into the KUKA robot's E6POS structure, which encapsulates a complete six-dimensional pose comprising both position and orientation. The ZYX Euler angles (*roll*, *pitch*, *yaw*), derived from the local surface frame, are directly mapped to the A, B, and C components of the E6POS structure, respectively. This enables the robotic arm to follow the adhesive path with precise orientation control, ensuring that the fixed spray head remains perpendicular to the shoe surface throughout the operation.

5. Experimental Results

 doi:10.20944/preprints202504.1336.v1

The overall lasted upper gluing system was developed using Microsoft Visual Studio 2022 as the programming environment, with C# as the implementation language. For image and point cloud processing, the system integrates OpenCvSharp and the Point Cloud Library (PCL) to construct 3D models of the shoe components. Four KUKA six-axis robotic arms were employed in the system, communicating through EKI (Ethernet KRL Interface) and KUKA's proprietary communication protocols. Robotic control was achieved using KUKA Robot Language (KRL) in combination with external control mode.

To evaluate the feasibility of the proposed automated gluing system under realistic production conditions, a comprehensive implementation test was conducted using a sports casual shoe produced by Fulgent Sun Group for the Swiss brand On, as illustrated in Figure 22. The upper of this shoe features smooth yet irregular surface curvatures. Since the bonding line of the lasted upper is defined by the edge contour of the outsole wall, any height variation along the outsole wall directly affects the position and geometry of the bonding line on the upper.

In traditional manual adhesive application, the outsole is first temporarily pressed against the lasted upper, allowing the operator to trace a bonding line along the edge of the outsole wall. Adhesive is then applied manually to the region below this line. To automate this process, the system must first identify the bonding line equivalent to that drawn manually. As described in previous sections, this is achieved by constructing accurate 3D models of the lasted upper and outsole, aligning them in 3D space, and generating the adhesive spraying path accordingly.

By integrating the proposed 3D modeling and path planning method with appropriate mechanical design, the automated gluing process was implemented across three sequential stages: (1) loading/initial drying and 3D scanning, (2) treatment agent and adhesive spraying, and (3) final drying and bonding. The implementation details of these three stages, along with corresponding results and observations, are presented in the following subsections.

Figure 22. Appearance of the On sports and casual shoes for verification.

5.1. Front Stage: Loading/Drying and 3D Scanning

The appearance of the first operational stage is shown in Figure 23. The process begins with placing the lasted upper onto the loading station, which then advances and enters the first drying oven for preliminary treatment, as illustrated in Figure 24a. Upon completion of the drying process, the lasted upper is transferred to the 3D scanning station via a motorized platform. There, it is gripped, rotated, and repositioned to initiate scanning, as shown in Figure 24b.

Once the lasted upper is properly positioned, the main control system triggers the 3D scanning system to perform a three-sided scan of the object—capturing the left, right, and top views simultaneously—as depicted in Figure 24c. During scanning, the system also determines the shoe size and left/right foot orientation. This information is concurrently transmitted to the outsole gluing line's preparation section, allowing a matching outsole to be prepared for gluing in advance. Such coordination ensures proper alignment and seamless bonding after the lasted upper has completed adhesive application and final drying.

 doi:10.20944/preprints202504.1336.v1

After the adhesive spraying path is constructed based on the scanned 3D model, the lasted upper is placed onto a rotary table by the scanning platform. It is then ready to be transferred to the next stage of the process, as illustrated in Figure 24(d).

Figure 23. External view of the loading/drying and 3D scanning station.

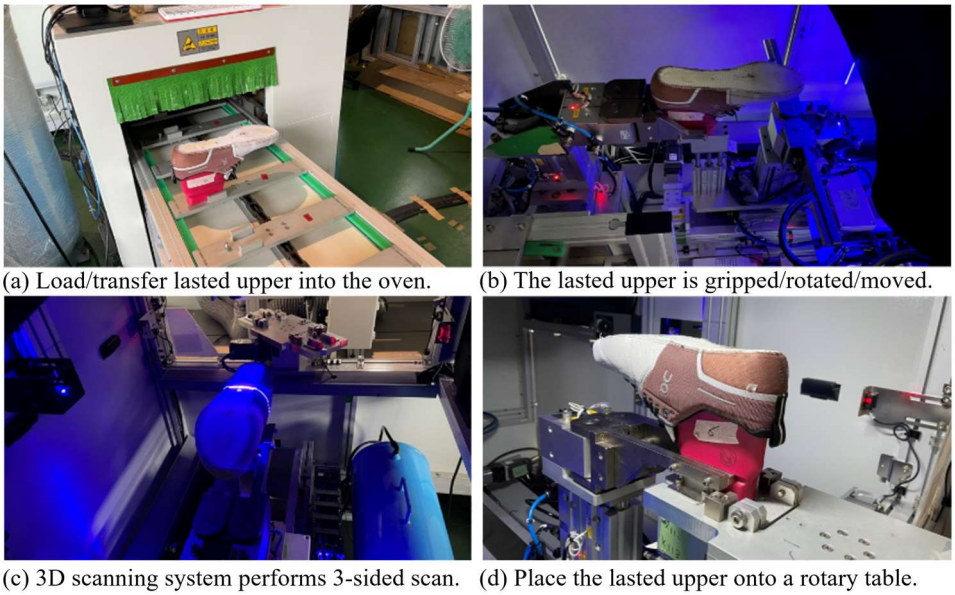
(a) Load/transfer lasted upper into the oven. (b) The lasted upper is gripped/rotated/moved.

(c) 3D scanning system performs 3-sided scan. (d) Place the lasted upper onto a rotary table.

Figure 24. Mechanical structure of the loading/drying and 3D scanning station.

5.2. Middle Stage: Treatment Agent and Water-Based Adhesive Spraying Station

After completing the 3D scanning process and generating the corresponding spraying path in the previous station, the lasted upper proceeds directly to the second stage, where a treatment agent (primer) and water-based adhesive are sequentially applied. This spraying station is operated by four six-axis robotic arms, arranged in two parallel pairs—one pair dedicated to spraying the treatment agent, and the other to spraying the adhesive.

The external appearance of this station is shown in Figure 25, where the lasted upper enters from the right side and exits on the left. The reason for pairing the robotic arms is to accommodate the higher processing speed of the outsole gluing line. To keep pace with the outsole process, the system assigns the left and right lasted uppers to separate robotic arms immediately after scanning. This setup enables near-concurrent spraying of both sides, thereby maintaining an efficient production flow without bottlenecks. The treatment agent is applied by the following steps:

1. The lasted upper (L.U.) is first transferred via a rotary table, where it is rotated and tilted in

 doi:10.20944/preprints202504.1336.v1

preparation for being gripped by the robotic arm at the primer station, as shown in Figure 26a.

2. The robotic arm then grips the shoe last, maneuvers it close to the fixed spray head, and follows the spraying path generated in the previous station to apply the treatment agent, as illustrated in Figure 26b.
3. Upon completion of the treatment agent spraying, the robotic arm places the lasted upper onto a supporting mechanism, as shown in Figure 26c.
4. Once the lasted upper is laid flat, a transfer mechanism grips the shoe last and places it onto the conveyor system, as depicted in Figure 26(d). The lasted upper is then conveyed into the oven to undergo the second drying stage.

After completing the second drying stage, the lasted upper is sequentially transferred to the water-based adhesive spraying station. This station adopts the same robotic configuration as the treatment agent station, with a pair of six-axis robotic arms responsible for spraying the left and right lasted uppers, respectively. The robotic arms grip the shoe last, maneuver it close to the fixed adhesive spray head, and follow the previously planned spraying path to apply the water-based adhesive.

The spraying process mirrors that of the treatment agent station in both sequence and motion control. However, due to the viscosity and transparency of the water-based adhesive, special attention is given to ensure consistent coating coverage. After the spraying is complete, the lasted upper is placed onto a supporting platform and then transferred onto the conveyor system for the final drying stage in the shared oven.

Figure 25. External view of the treatment agent and adhesive spraying station.

 doi:10.20944/preprints202504.1336.v1

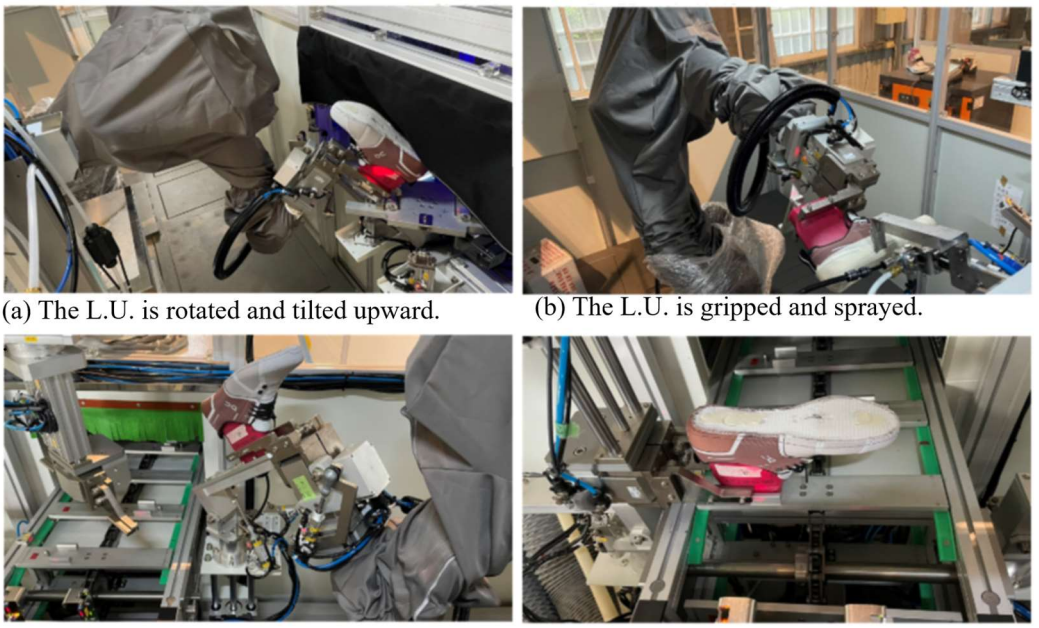

Figure 26. Steps of the treatment agent spraying process.

5.3. Final Stage: Final Drying and Bonding

After the water-based adhesive is applied, the transfer mechanism places the lasted upper onto the conveyor system, which transports it into the oven for the final drying stage, as depicted in Figure 27. At the same time, the corresponding outsole is also sent into the same oven. This shared oven is designed with two layers:

- The upper layer receives the glued outsoles from the outsole line.
- The lower layer processes the matched lasted uppers.

The dual-layer structure enables parallel thermal treatment of both components while maintaining alignment between the matched pairs. Once drying is complete, the system transfers the lasted upper and its corresponding outsole to the bonding station, where manual assembly is used to attach the two components. This manual step is currently retained to ensure precise alignment, effective pressure application, and to allow for manual stretching of the upper to fit the contour of the outsole. In addition, the operator is able to remove excess adhesive (overflow) and fill in any uncovered areas (underfill) as needed, ensuring bonding quality before final setting. The entire gluing and bonding process is thereby completed.

 doi:10.20944/preprints202504.1336.v1

Figure 27. External view of the shared oven and the bonding area for upper–outsole assembly.

5.4. Summary of Experimental Results

The experimental implementation of the proposed lasted upper gluing system demonstrated the feasibility of integrating 3D vision, robotic path planning, and multi-stage adhesive application within a real production environment. Through a structured three-stage process—comprising initial drying and scanning, treatment agent and adhesive spraying, and final drying and bonding—the system successfully automated a traditionally manual process. Each robotic station performed precise manipulation and spraying based on customized 3D path planning, while synchronization with the outsole line ensured seamless assembly preparation.

Although the final bonding step is currently performed manually to accommodate variability in shoe profiles and ensure alignment accuracy, the system layout has been designed with future robotic integration in mind. Overall, the results validate the system's ability to support flexible and efficient adhesive application for footwear manufacturing.

6. Performance Evaluation and Discussion

To validate the practical performance of the proposed lasted upper gluing system, a series of experimental evaluations were conducted. While the previous section focused on the step-by-step implementation of the multi-stage process, this section presents a comprehensive assessment of the system's effectiveness, operational efficiency, and quantitative outcomes.

Specifically, the following aspects are analyzed:

(1) The quality and accuracy of the adhesive spraying results,

(2) The time consumption and throughput of the gluing process, and

(3) The system's overall performance in terms of precision, repeatability, and coverage consistency.

Through this evaluation, we aim to verify the reliability of the proposed approach and identify practical limitations or areas for future improvement.

6.1. Adhesive Spraying Results

Since the water-based adhesive is transparent, its presence is not visually detectable after application. To enable inspection and verify whether the adhesive coverage meets process requirements, a UV fluorescent dye was added to the adhesive formulation. After the spraying process, a UV lamp was used to illuminate the lasted upper, allowing the adhesive-covered regions to fluoresce and thus reveal the actual coverage.

To evaluate whether the adhesive was accurately applied along the intended bonding area, a reference bonding line was manually drawn on each lasted upper prior to the spraying process, following the traditional method used in manual gluing. This line served as the baseline for comparing the sprayed adhesive coverage with the expected bonding region.

The adhesive coverage, visualized under UV light due to the added fluorescent dye, is shown in Figure 28. As illustrated, the adhesive applied to the toe, heel, and both lateral sides of the lasted upper closely follows the manually defined bonding lines. This outcome confirms that the system has successfully completed customized path planning for each individual lasted upper. Moreover, it demonstrates that the robotic arm precisely executed the spraying motion along the planned trajectory, achieving accurate and consistent adhesive application.

In the footwear industry, a deviation of less than 1 mm from the bonding line is generally considered acceptable. Based on the inspection images, nearly all regions of the adhesive application fall within this tolerance range—except for a small area at the toe cap, where slight deviation is observed. This particular issue will be discussed in detail in the following section.

 doi:10.20944/preprints202504.1336.v1

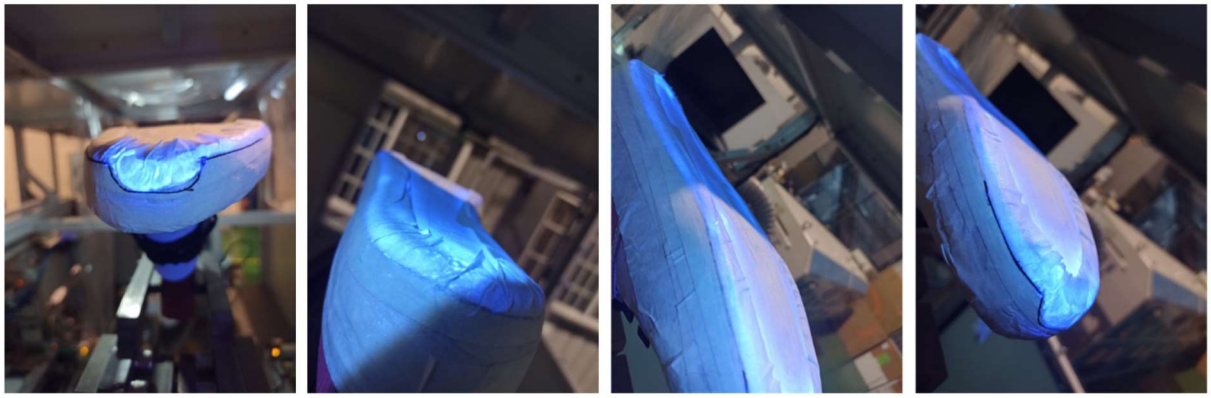

Figure 28. UV-based verification of adhesive spraying results. The fluorescent dye enables visualization of adhesive coverage under UV light. From left to right: toe, heel, left side, and right side. The sprayed adhesive closely follows the bonding lines, with slight deviation observed at the toe.

6.2. Gluing Process Time Analysis

The total time required to complete the gluing process—from the point at which the lasted upper enters the first drying oven to its exit from the final oven and arrival at the bonding station—is approximately 580 seconds. The time consumed by each process stage is detailed in Table 1.

- The first drying stage takes approximately 60 seconds.
- The 3D scanning and transportation process requires around 10 seconds.
- Each pick-and-place operation for the lasted upper takes approximately 15 seconds, with a total of seven such operations throughout the entire process (105 s in total).
- Each spraying operation—for both treatment agent and adhesive—takes about 45 seconds.
- The second and third drying stages are the most time-consuming, requiring 180 seconds each.

From the data in Table 1, it is evident that the drying stages account for the majority of the process time. However, since these stages are critical to ensure complete adhesive curing, their durations are fixed and cannot be shortened without compromising process quality.

To maintain full production efficiency, the system ensures that each carrier on the conveyor is consistently loaded with a lasted upper. The robotic arm operations are synchronized with the conveyor speed and adapt to the required motion times. Although a single lasted upper requires nearly 10 minutes to complete the full process, the system operates in a pipeline workflow, where multiple stages are executed in parallel. This allows the system to maintain a cycle time of approximately one pair per minute during continuous operation.

Based on this cycle time and the use of dual parallel spraying lines—handling left and right lasted uppers separately—the system can achieve an estimated throughput of up to 1000 pairs of shoes in a standard 8-hour workday. This output aligns well with practical manufacturing expectations and validates the proposed system's suitability for industrial-scale production.

Table 1. Time consumption of each stage in the lasted upper gluing process. The total cycle time is optimized through pipeline synchronization, while the drying stages remain fixed due to adhesive curing requirements.

Process Stage	Time (seconds)
First drying (1st Oven)	60
3D scanning and transport	10
Pick and Place of the lasted upper ×7	15 x 7 = 105

 doi:10.20944/preprints202504.1336.v1

Spraying Operation ×2	45
Second drying (2nd Oven)	180
Third drying stage (3rd Shared Oven)	180
Total process time	580

6.3. Quantitative Performance and Discussion

To ensure dimensional accuracy in the adhesive spraying process, the displacement-to-height conversion curves derived in Section 4.1.3 were implemented on the production line using a custom-built three-level calibration block, as shown in Figure 29. Calibration tests yielded average measurement errors of approximately 0.34 mm on the left side, 0.35 mm on the right side, and 0.13 mm on the top. These deviations are minimal and fall well within acceptable limits for adhesive path planning.

To further evaluate the repeatability of the height measurements, a lasted upper of a fixed size was repeatedly scanned, focusing on the left and right side regions. The deviations from the average value were observed to lie within the range of −0.4 mm to +0.5 mm. Such variations are considered negligible in the context of footwear adhesive application and do not compromise process quality. These deviations are significantly below the generally accepted tolerance of ±1 mm in industrial footwear manufacturing, thereby confirming the suitability of the 3D scanning and height mapping system for practical adhesive path planning.

In practical tests, these measured deviations were found to have no adverse effect on spraying performance. The robotic arm was consistently able to maintain proper positioning and stable contact pressure between the lasted upper and the spraying guide plate. As a result, the adhesive was applied accurately and uniformly, confirming that the proposed system delivers reliable coating performance despite minor variations in height measurements.

While the overall adhesive application meets industrial standards, a localized glue-deficient area was observed near the toe cap, as shown in Figure 28. This issue arises from the inability of the spraying mechanism to perfectly follow the bonding line in regions with high curvature—particularly the sharp arc at the front of the shoe.

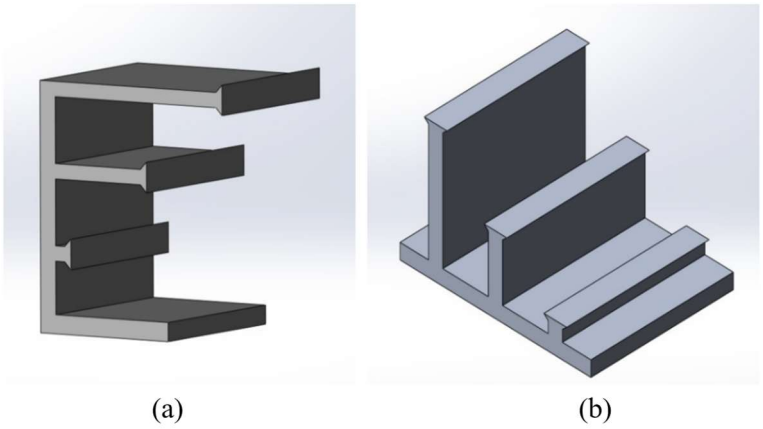

Figure 29. Calibration fixtures for 3D scanning system: (a) fixture used for left and right. (b) Fixture used for top.

As illustrated in Figure 29, when the robotic arm moves the lasted upper past the fixed spray head, the straight lower edge of the baffle fails to conform to the rounded geometry of the toe cap. This causes adhesive to overflow beyond the intended bonding line. To mitigate this issue, the spraying path was adjusted slightly inward along the bonding line to minimize overflow. However, this adjustment resulted in the baffle partially obstructing the inner edge of the bonding area, leading to localized glue deficiency.

 doi:10.20944/preprints202504.1336.v1

This trade-off between preventing overflow and avoiding undercoverage highlights a design limitation of the current baffle geometry when dealing with complex curves. Further improvements—such as adopting a more flexible or curved baffle design, or integrating dynamic nozzle orientation—may help resolve this issue in future system iterations.

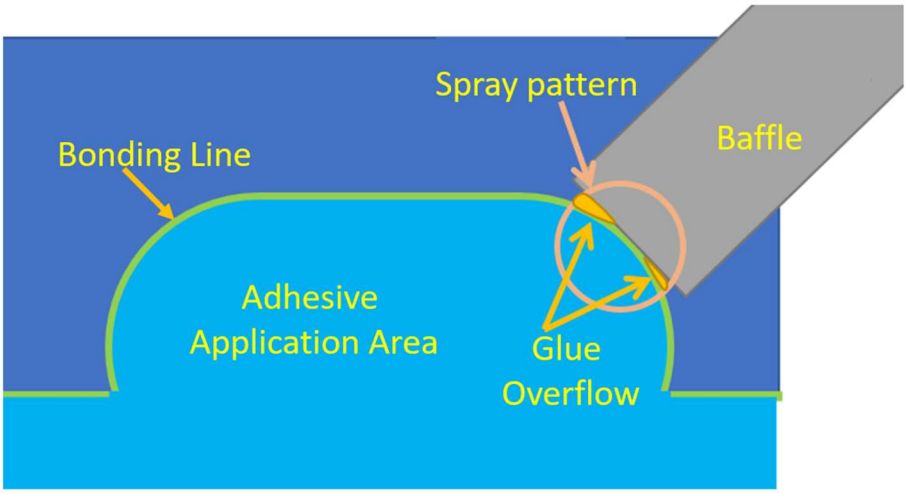

Figure 29. Glue overflow observed at the toe cap, caused by a mismatch between the curved bonding line and the straight geometry of the spray baffle. This geometric misalignment results in excess adhesive beyond the bonding area when spraying over sharp arcs..

7. Conclusions

This study presents a fully automated lasted upper gluing system that integrates 3D computer vision, six-axis robotic arms, a fixed spraying mechanism, thermal ovens, and synchronized peripheral devices. The system successfully achieves its intended goal of automating the traditionally manual process of applying primer and water-based adhesive to footwear uppers.

By employing a custom-built 3D scanning platform, each lasted upper is digitally reconstructed in real-time, allowing the system to generate customized adhesive spraying paths tailored to individual shoe geometries. These paths are then executed by robotic arms with high repeatability and stable orientation control, resulting in accurate and consistent adhesive application. The system not only reduces labor requirements and improves production efficiency but also eliminates manual tasks that often pose ergonomic risks to workers on the factory floor.

Experimental validation confirms the accuracy of height measurement and spraying precision. Most adhesive application results remained within an acceptable deviation of ±1 mm, meeting industrial standards. While localized deviations—particularly around the toe cap—were observed due to mismatches between the fixed baffle geometry and the curved bonding line, these remain within an acceptable range and provide direction for future system enhancements.

Future work will focus on improving the system's adaptability to complex geometries. This includes optimizing the baffle design, refining robotic trajectory planning in high-curvature regions, and introducing potential real-time adjustment mechanisms. Additionally, efforts will be made to further reduce cycle time and energy consumption by fine-tuning the synchronization between spraying, drying, and transfer stages. These improvements are expected to enhance spraying accuracy in high-curvature areas—such as the toe cap—while increasing throughput and maintaining high coating quality. Ultimately, these enhancements aim to deliver a robust and intelligent adhesive application system that not only improves spraying accuracy in complex regions but also supports scalable deployment in real-world production lines—such as the one successfully implemented and validated in Hanoi, Vietnam.

 doi:10.20944/preprints202504.1336.v1

Acknowledgements: This work was supported by Fulgent Sun Group, whose contributions went beyond funding by also providing essential sample materials and valuable access to field testing environments. The authors would like to express their sincere gratitude for this generous support. Special thanks are also extended to Sheng Yu Co., Ltd. for their long-term assistance in mechanical design and production line implementation, which played a critical role in bringing the system into practical use.

References

1. Wei, Y.H.D. China's Shoe Manufacturing and the Wenzhou Model: Perspectives on the World's Leading Producer and Exporter of Footwear. *Eurasian Geogr. Econ.* **2009**, *50*, 720–739. https://doi.org/10.2747/1539-7216.50.6.720.
2. Maurtua, I.; Ibarguren, A.; Tellaeche, A. Robotics for the Benefit of Footwear Industry. In *Intelligent Robotics and Applications*; Su, C.-Y., Rakheja, S., Liu, H., Eds.; Springer: Berlin/Heidelberg, Germany, 2012; Volume 7507, pp. 235–244. https://doi.org/10.1007/978-3-642-33515-0_24.
3. Nike and Flex to End Partnership. Available online: https://sgbonline.com/nike-and-flex-to-end-partnership/ (accessed on 8 April 2025).
4. Kim, J.Y. CAD-based Automated Robot Programming in Adhesive Spray Systems for Shoe Outsoles and Uppers. *J. Robot. Syst.* **2004**, *21*, 625–634. https://doi.org/10.1002/rob.20040.
5. Castelli, K.; Zaki, A.M.A.; Dmytriyev, Y.; Carnevale, M.; Giberti, H. A Feasibility Study of a Robotic Approach for the Gluing Process in the Footwear Industry. *Robotics* **2020**, *10*, 6. https://doi.org/10.3390/robotics10010006.
6. Kim, M.-G.; Kim, J.; Chung, S.Y.; Jin, M.; Hwang, M.J. Robot-Based Automation for Upper and Sole Manufacturing in Shoe Production. *Machines* **2022**, *10*, 255. https://doi.org/10.3390/machines10040255.
7. Wu, J.; Zhu, K. An Algorithm for Extracting Spray Trajectory Based on Laser Vision. In Proceedings of the 2017 IEEE International Conference on Communication Technology (ICCT), Chengdu, China, 27–30 October 2017; pp. 1591–1595. https://doi.org/10.1109/ICCT.2017.8359899.
8. Oliver, G.; Gil, P.; Torres, F. Robotic Workcell for Sole Grasping in Footwear Manufacturing. In Proceedings of the 2020 25th IEEE International Conference on Emerging Technologies and Factory Automation (ETFA), Vienna, Austria, 8–11 September 2020; pp. 704–710. https://doi.org/10.1109/ETFA46521.2020.9212058.
9. Gu, Z.; Liu, X.; Wei, L.; Huang, Y.; Sheng, X. Shoe Sole Contour Extraction Based on Two-Dimensional Maximum Entropy Threshold Segmentation. In Proceedings of the 2021 40th Chinese Control Conference (CCC), Shanghai, China, 26–28 July 2021; pp. 6568–6573. https://doi.org/10.23919/CCC52363.2021.9549780.
10. Song, L.; Luo, J.; Wen, Y. Intelligent Three-Dimensional Shape Recovery System for Shoes. In Proceedings of the 2009 International Workshop on Intelligent Systems and Applications, Wuhan, China, 23–24 May 2009; pp. 1–4. https://doi.org/10.1109/IWISA.2009.5072926.
11. Wu, C.; Ni, Y.; Li, Q.; Jin, Y. Implementation of 5-DOF Apparatus Used for Adhesive Spray and Roughing of Shoe Upper. In Proceedings of the 2008 IEEE International Conference on Automation and Logistics, Qingdao, China, 1–3 September 2008; pp. 1408–1413. https://doi.org/10.1109/ICAL.2008.4636374.
12. Wu, C.; Mao, X.; Shi, X.; Zhang, L. Methods of Generating Robot Spraying Trajectory Based on Shoe Sole Information. In Proceedings of the 2009 International Workshop on Intelligent Systems and Applications, Wuhan, China, 23–24 May 2009; pp. 1–4. https://doi.org/10.1109/IWISA.2009.5072953.
13. Jin, Y.; Zhang, L.; Wu, C.; Zhu, Z. Detection of 3D Curve for Shoe Sole Spraying Based on Laser Triangulation Measurement. In Proceedings of the 2009 IEEE International Conference on Automation and Logistics, Shenyang, China, 5–7 August 2009; pp. 865–868. https://doi.org/10.1109/ICAL.2009.5262802.
14. Hu, Z.; Bicker, R.; Taylor, P.; Marshall, C. Computer Vision for Shoe Upper Profile Measurement via Upper and Sole Conformal Matching. *Opt. Lasers Eng.* **2007**, *45*, 183–190. https://doi.org/10.1016/j.optlaseng.2006.04.004.
15. Wu, X.; Li, Z.; Wen, P. An Automatic Shoe-Groove Feature Extraction Method Based on Robot and Structural Laser Scanning. *Int. J. Adv. Robot. Syst.* **2017**, *14*, 1–12. https://doi.org/10.1177/1729881416678135.
16. Pagano, S.; Russo, R.; Savino, S. A Vision Guided Robotic System for Flexible Gluing Process in the Footwear Industry. *Robot. Comput.-Integr. Manuf.* **2020**, *65*, 101965. https://doi.org/10.1016/j.rcim.2020.101965.

 doi:10.20944/preprints202504.1336.v1

17. Lee, C.-Y.; Kao, T.-L.; Wang, K.-S. Implementation of a Robotic Arm with 3D Vision for Shoes Glue Spraying System. In Proceedings of the 2018 2nd International Conference on Computer Science and Artificial Intelligence (CSAI), Shenzhen, China, 8–10 December 2018; pp. 562–565. https://doi.org/10.1145/3297156.3297171.
18. Gómez-Hernández, J.-F.; Gutiérrez-Hernández, J.-M.; Jimeno-Morenilla, A.; Sánchez-Romero, J.-L.; Fabregat-Periago, M.-D. Development of an Integrated Robotic Workcell for Automated Bonding in Footwear Manufacturing. *IEEE Access* **2024**, *12*, 5066–5080. https://doi.org/10.1109/ACCESS.2024.3350441.
19. Hou, X.; Li, J. 3-D Trajectory Planning Scheme for Shoe Upper Processing. *IEEE Trans. Instrum. Meas.* **2024**, *73*, 1–15. https://doi.org/10.1109/TIM.2024.3476594.
20. Blais, F. Review of 20 Years of Range Sensor Development. *J. Electron. Imaging* **2004**, *13*, 231. https://doi.org/10.1117/1.1631921.
21. Franca, J.G.D.M.; Gazziro, M.A.; Ide, A.N.; Saito, J.H. A 3D Scanning System Based on Laser Triangulation and Variable Field of View. In Proceedings of the IEEE International Conference on Image Processing, Genova, Italy, 11–14 September 2005; pp. I–425. https://doi.org/10.1109/ICIP.2005.1529778.
22. Jin, Y.; Zhang, L.; Wu, C.; Zhu, Z. Detection of 3D Curve for Shoe Sole Coating Based on Laser Triangulation Measurement. In Proceedings of the 2009 IEEE International Conference on Automation and Logistics, Shenyang, China, 5–7 August 2009; pp. 865–868. https://doi.org/10.1109/ICAL.2009.5262802.
23. Rusu, R.B.; Cousins, S. 3D Is Here: Point Cloud Library (PCL). In Proceedings of the 2011 IEEE International Conference on Robotics and Automation, Shanghai, China, 9–13 May 2011; pp. 1–4. https://doi.org/10.1109/ICRA.2011.5980567.
24. Suzuki, S.; Be, K. Topological Structural Analysis of Digitized Binary Images by Border Following. *Comput. Vis. Graph. Image Process.* **1985**, *30*, 32–46.